

NODIS: Neural Ordinary Differential Scene Understanding

Cong Yuren¹, Hanno Ackermann¹, Wentong Liao¹, Michael Ying Yang², and Bodo Rosenhahn¹

¹Leibniz University Hannover, Germany

²Twente University, The Netherlands

Abstract

Semantic image understanding is a challenging topic in computer vision. It requires to detect all objects in an image, but also to identify all the relations between them. Detected objects, their labels and the discovered relations can be used to construct a scene graph which provides an abstract semantic interpretation of an image. In previous works, relations were identified by solving an assignment problem formulated as Mixed-Integer Linear Programs. In this work, we interpret that formulation as Ordinary Differential Equation (ODE). The proposed architecture performs scene graph inference by solving a neural variant of an ODE by end-to-end learning. It achieves state-of-the-art results on all three benchmark tasks: scene graph generation (SGGen), classification (SGCls) and visual relationship detection (PredCls) on Visual Genome benchmark.

1. Introduction

This paper investigates the problem of semantic image understanding. Given an image, the objective is to detect objects within, label them and infer the relations which might exist between objects. These data provide rich semantic information about the image content. So called scene graphs contain all these information and constitute abstract representations of images [9]. Nodes of a scene graph represent objects detected in an image, while edges represent relationships between objects, for instance the *object-predicate-object* triplet *window-on-bus* as shown in Fig. 1. Applications range from image retrieval [9] to high-level vision tasks such as visual question answering [29], image captioning [38, 35] and visual reasoning [26]. The community has been very active in the past years to investigate this and related problems such as visual relationship detection. Results on benchmark problems like the Visual Genome database [12] have improved drastically within the past few years [32, 40, 2].

A naive approach to infer scene graphs is to use a stan-

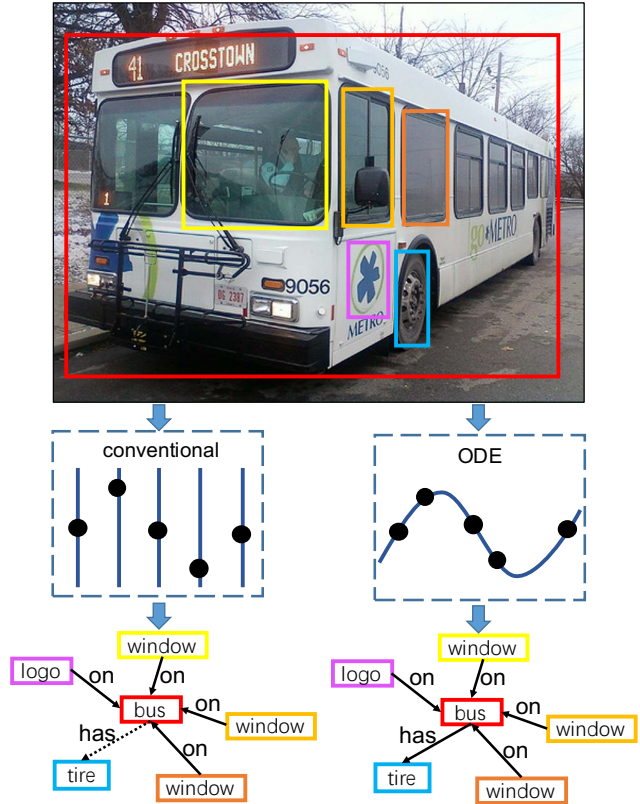


Figure 1: Visualization of main contributions made in this work. State-of-the-art works rely on multiple embedding layers which amounts to an evenly-spaced, discrete sampling whereas the proposed module relies on ordinary differential equations (ODE), thus it learns a continuous approximation of the trajectory onto the embedding manifolds.

dard object detector, classify the objects, and use a separate network to label the relationships between the objects. This, however, ignores the conditional information shared between the objects. It has therefore become standard prac-

tice to also use relationship information for object classification [8, 20, 17].

A noteworthy feature of state-of-the-art works such as [33, 40] is that all employ end-to-end training, i.e. every component of the pipeline is differentiable. On the other hand, labels and assignments were estimated by solving a Mixed-Integer Linear Program (MILP) in [27]. This makes MILPs potentially useful tools for scene graph estimation. However, the disadvantage of using MILPs is that end-to-end learning is no longer possible since MILP solvers include steps which are non-differentiable, hence backpropagation cannot be used for pipelines including them.

For many other problems in which backpropagation into previous steps of pipelines is less important, MILPs have been successfully employed. In [6], network flows and transport problem were modeled by Partial Differential Equations (PDEs). The arising systems of PDEs are simplified to systems of Ordinary Differential Equations (ODEs) by finite differences. Finally, optimal solutions are obtained by solving MILPs which further include optimization objectives. That implies that for properly constructed MILPs there are systems of ODEs¹ which include the solution of the MILPs. While backpropagating through an MILP is generally not possible, backpropagation through an ODE is possible using *Neural Ordinary Differential Equations* which were recently proposed in [3].

In this paper, we will use this link for an end-to-end trainable network. The assignment problems to infer visual relationships are not solved by MILPs but by *learning* neural implementations of ordinary differential equations using [3]. Thereby, we learn the optimal function to solve the assignment problem which is an integral part of visual relationship detection, yet avoid the necessity to backpropagate through an MILP. In contrast, state-of-the-art works use ad-hoc architectures to solve the assignment problem. The proposed network is end-to-end trainable². We show state-of-the-art results in all three benchmark problems: scene graph generation (SGGen), scene graph classification (SGCls) and visual relationship prediction (PredCls). A variant of our model is evaluated as the second best model, outperforming state-of-the-art algorithms on several tasks.

The **contributions** made in this work can be summarized as follows:

- We propose to use a neural ordinary differential equation (ODE) network for scene graph generation. It learns the optimal assignment function whereas previous works use ad-hoc networks for that purpose.
- Direct end-to-end training, easier than message passing schemes.

¹This mapping usually is one-to-many.

²The code and a pre-trained model will be published on GitHub.

- The best proposed method achieves state-of-the-art results. The second best proposed method is superior to existing works in several categories.

This paper is structured as follows: In Sec. 2, we briefly summarize related works. In Sec. 3, we introduce the proposed architecture. Quantitative and qualitative results are shown in Sec. 5. Finally, we conclude this paper in Sec. 6.

2. Related Work

Context for Visual Reasoning: Context has been used in semantic image understanding [5, 14, 37, 8, 20]. For scene graph generation, context information has been recently proposed and is still being investigated. Message passing has been used to include object context in images in several works, for instance by graphical models [16, 33], by recurrent neural networks (RNN) [40, 30], or by an iterative refinement process [32, 11]. Context from language priors [22] has been proved to be helpful for visual relationships detection and scene graph generation [21, 39, 17].

Scene Graph Generation: Scene graphs are proposed in [9] for the task of image retrieval. They consist of not only detected objects but also the object classes and the relationships between the detected objects. The estimation of scene graphs from images is drawing increasing attention in computer vision [17, 4, 18, 42, 16, 40, 30]. Several of these methods use message passing to capture the context of the two related objects [15, 40, 30], or of the objects and their relationships [32, 17, 16, 33]. The general pipeline for message passing is to train some shared matrices to transform the source features into a semantic domain and then to assemble them to update the target features. In some works, an attention mechanism is implemented to weight the propagated information to achieve further improvement [16, 33]. Graph CNNs [10] have been used to propagate information between object and relationship nodes [33].

Contrastive Training: Contrastive losses [1] have been applied for scene understanding [41]. They have also been applied for image captioning, visual question answering (VQA) and vector embeddings [36, 23, 25]. They are based on the idea that it can be easier to select which samples are definitely from a different class than to obtain labels. In other words, such losses can be used when no label information is available.

Losses: In Visual Genome [12], most semantically meaningful relations are not labelled. Furthermore, relations that can have multiple labels, for instance `on` and `sit`, are usually labelled only once. Networks for visual relationship detection which use cross-entropy as training loss may encounter difficulties during training, since almost identical pairs of objects can have either label, or even none at all. To overcome the problem of such contradicting label information, margin-based [13] and contrastive [41] losses have

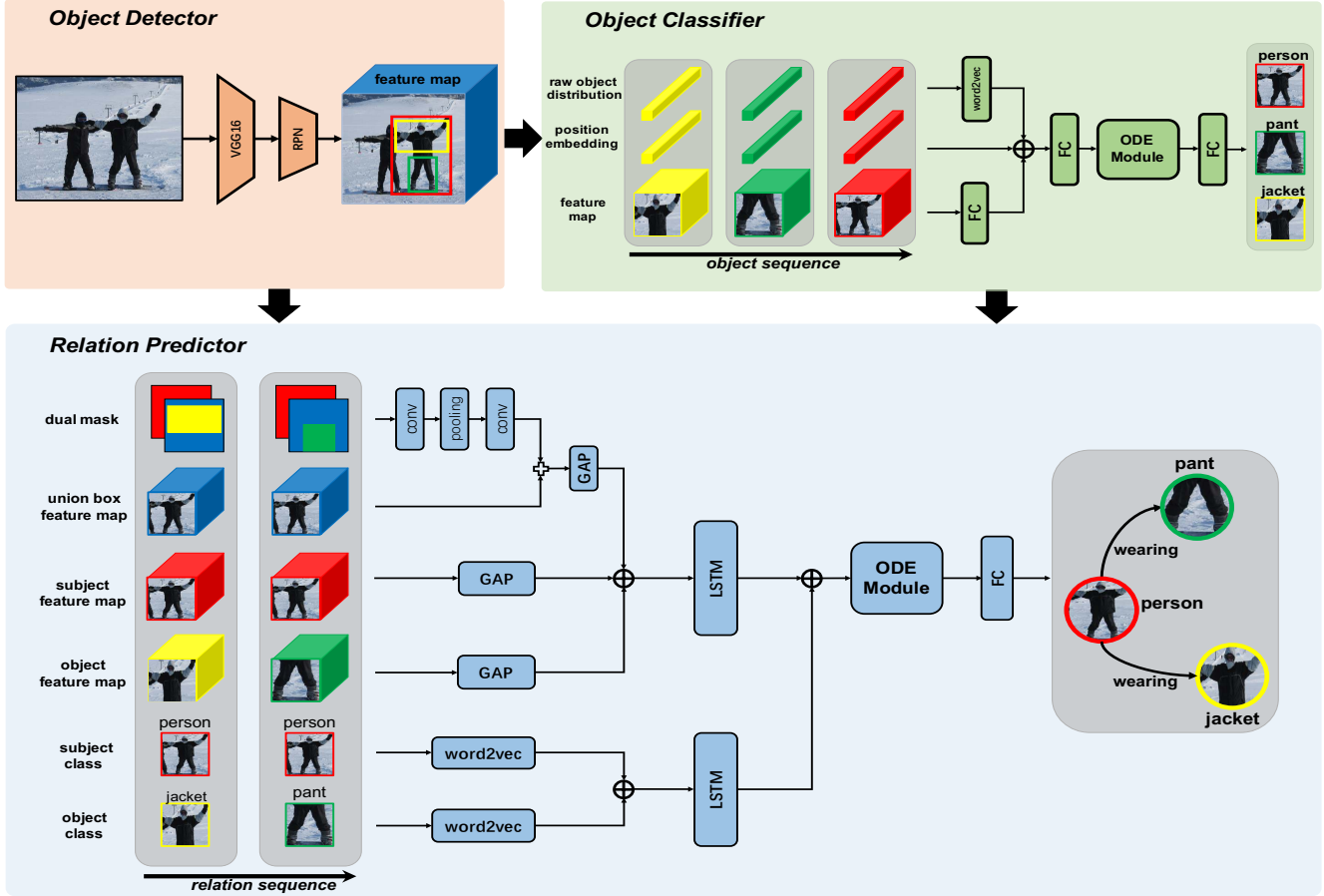


Figure 2: Overview of proposed architecture (best viewed in color). The orange block in the upper left corner serves as object detector and corresponds to $P(\mathcal{B}|\mathcal{I})$ (cf. Sec. 3.3). The green block in the upper right corner depicts the structure of the object detector, $P(\mathcal{O}|\mathcal{B}, \mathcal{I})$. The blue bloc in the lower half shows the relationship classifier, $P(\mathcal{R}|\mathcal{O}, \mathcal{B}, \mathcal{I})$. In contrast to previous works on semantic image understanding, the proposed neural architecture includes ordinary differential equation (ODE) modules in the object and the relationship classifiers. GAP is the abbreviation of global average pooling.

been proposed.

Support Inference: Inferring physical support, i.e. which structures for instance carry others, e.g. `floor` \rightarrow `table`, was investigated for object segmentation [27], instance segmentation [43], and also for scene graph inference [34].

Proposed model: The proposed model uses neither iterations, except for LSTM-cells, nor message passing, nor a Graph CNN. As most recent works do, language priors are included. We further use a standard loss based on cross-entropy. Unlike most state-of-the-art algorithms, we propose using a new module which has never before been used for semantic image analysis. The ODE module [3] can be interpreted as learning a deep residual model. In contrast to residual networks, the ODE-module *continuously* models its solutions according to a pre-defined, problem-specific precision.

This idea is motivated by works on gas, water, energy

and transport networks which need to be modeled by systems of Partial Differential Equations (PDE). In [6], it was proposed to simply such system to obtain systems of Ordinary Differential Equations (ODE), add one or multiple optimization objectives and then use a Mixed-Integer Linear Program to compute the solution. That implies that, given an MILP, we can always find a system of ODEs that can generate the same solution among others. Using a neural ODE [3], we can thus learn a function of the system of ODEs.

Summarizing, state-of-the-art works define the final assignment networks ad-hoc³, whereas we learn the optimal function to perform that operation⁴.

³This is otherwise known as *grad student descent*.

⁴The purpose of the final fully connected layers which follow the ODE modules is only to compute class scores for the cross-entropy loss, see Fig.2.

3. Model

In this section, we first define scene graphs, before we briefly review Neural Ordinary Differential Equations presented in [3]. We define the statistical model that we assume for scene graph generation in Sec. 3.3. The proposed ODE-based blocks for object and relationship classification are introduced in Secs. 3.5 and 3.6.

3.1. Scene Graphs

A scene graph $G \in (o_i \times r_k \times o_j)$ [9] is an abstract semantic representation of all objects in an image and the relationships between them. The set of objects $\mathcal{O} = (o_1, \dots)$ consists of a set of bounding boxes $\mathcal{B}_{\mathcal{O}} = (b_{\mathcal{O},1}, \dots)$ along with labels $\mathcal{L} = (l_1 \dots l_N)$ with N indicates the total number of different objects. The set of relationships, also known as predicates, $\mathcal{R} = (r_1, \dots)$ consists of bounding boxes $\mathcal{B}_{\mathcal{R}} = (b_{\mathcal{R},1}, \dots)$ and labels $\mathcal{L} = (l_{N+1} \dots l_{N+K})$ where K denotes the number of different relations. As in [40], we include a particular predicate to indicate that there is no relation between two objects. Lastly, we are given sets of feature maps $\mathcal{F}_{\mathcal{O}}$ and $\mathcal{F}_{\mathcal{R}}$ for each bonding box.

3.2. Neural Ordinary Differential Equations [3]

Neural models f_{θ_k} with parameters k which include residual connections between layers k and $k+1$ map a signal x_k to x_{k+1} by

$$x_{k+1} = x_k + f_{\theta_k}(x_k). \quad (1)$$

This can be considered as a discrete approximation of the continuous dynamics of a model defined by ordinary differential equations (ODE) [3]

$$\frac{d}{dt}f = f(x(t), t, \theta). \quad (2)$$

Starting with an input $x(0)$ at time $t = 0$, the output at time T can be computed by a black-box ODE-solver. The dynamics of the system can thereby be approximated up to the required precision. Importantly, model states at times $0 < t < T$ need not be evenly spaced.

For backpropagation, the derivatives for the adjoint $a(t) = -\partial L / \partial x(t)$

$$\frac{d}{dt}a = -a(t)^\top \frac{\partial}{\partial t} f(x(t), t, \theta) \quad (3)$$

and

$$\frac{d}{d\theta}L = \int_T^0 a(t)^\top \frac{\partial}{\partial \theta} f(x(t), t, \theta) dt \quad (4)$$

have to be computed for loss L . This computation, along with the reverse computation of $x(t)$ starting at time T can be done by a single call of the ODE-solver backwards in time.

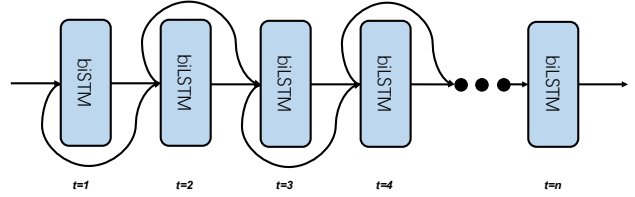


Figure 3: Bidirectional LSTM cells are used in the ODE solver so that the ODE module operates as a continuous deep residual bidirectional LSTM network.

3.3. Statistical Model

As in [40], we assume that the probability of a scene graph G given its image \mathcal{I} , $P(G|\mathcal{I})$, can be decomposed into three factors corresponding to the object detection model, given the image, $P(\mathcal{B}|\mathcal{I})$; the object classification model given image and bounding boxes, $P(\mathcal{O}|\mathcal{B}, \mathcal{I})$; and finally the relationship classification given image, bounding boxes and object classes, $P(\mathcal{R}|\mathcal{O}, \mathcal{B}, \mathcal{I})$:

$$P(G|\mathcal{I}) = P(\mathcal{B}|\mathcal{I})P(\mathcal{O}|\mathcal{B}, \mathcal{I})P(\mathcal{R}|\mathcal{O}, \mathcal{B}, \mathcal{I}). \quad (5)$$

The models of object detection $P(\mathcal{B}|\mathcal{I})$, object classification $P(\mathcal{O}|\mathcal{B}, \mathcal{I})$, and predicate classification $P(\mathcal{R}|\mathcal{O}, \mathcal{B}, \mathcal{I})$ are explained in Sections 3.4, 3.5 and 3.6, respectively.

3.4. Object Detection

Before reasoning about the scene graph, objects present in the given images must be localized as a set of candidate components of the relationships. To estimate the model of bounding boxes, $P(\mathcal{B}|\mathcal{I})$, as well as corresponding feature vectors and tentative object labels, we use a standard Faster R-CNN [24] with VGG16 [28] as backbone. The parameters of the Faster R-CNN are pre-trained and remain unchanged.

3.5. Object Classification

Object classification given bounding boxes and tentative labels can be formally stated as optimizing a mixed-integer assignment problem. In [6] it was shown how to solve an ordinary linear differential equation system by means of MILPs, hence, given an MILP, there exists an unknown ODE which can be solved by the MILP. Due to the large variability in natural image data, we do not intend to specify the ODE, but to *learn* its function as shown in [3].

As function approximator, we choose a recurrent neural network using LSTM-cells. This is motivated by the ability of the RNN-chain to model conditional probabilities between its inputs. Given a function $f_{\mathcal{O}}$ of the feature maps, a function $b'_{\mathcal{O}}$ of the bounding boxes of the object detections and a function $l'_{\mathcal{O}}$ of the tentative labels, we define the

neural ordinary equation model

$$\frac{d}{dt}f_{\mathcal{O}} = \text{biLSTM}(b'_{\mathcal{O}}, f_{\mathcal{O}}, l'_{\mathcal{O}}). \quad (6)$$

Intuitively, the model defined by Eq. (6) can be interpreted as deep residual LSTM-block, i.e. a stack of LSTM-chains with skip connections as in [31] (cf. Fig. 3). The precision parameter to evaluate the ODE-solver with can be thought of as continuously controlling the number LSTM-chains (cf. [3]).

Object class predictions are obtained by the hidden states obtained by solving Eq. (6)

$$P(\mathcal{O} | \mathcal{B}, \mathcal{I}) = W_{\mathcal{O}} [h_{\mathcal{O},1} \ \cdots \ h_{\mathcal{O},N}] + B_{\mathcal{O}}. \quad (7)$$

The matrices $W_{\mathcal{O}}$ and $B_{\mathcal{O}} = b_{\mathcal{O}}\mathbf{1}^{\top}$ define weights and biases of the classification layer.

Confer to the green box in the upper right corner of Fig. 2 for a schematic representation of the object classifier.

3.6. Relationships

Similarly as for object classification, we use the ODE-solver to learn a function that approximates an MILP. As neural network, we also choose an LSTM-model. Given a function $f_{\mathcal{R}}$ of the feature maps, a function $b'_{\mathcal{R}}$ of the bounding boxes of the relationship detections and a function $l'_{\mathcal{R}}$ of their tentative labels, we define

$$\frac{d}{dt}f_{\mathcal{R}} = \text{biLSTM}(b'_{\mathcal{R}}, f_{\mathcal{R}}, l'_{\mathcal{R}}). \quad (8)$$

Predicate class predictions are obtained by the hidden states obtained by solving Eq. (8)

$$P(\mathcal{R} | \mathcal{O}, \mathcal{B}, \mathcal{I}) = W_{\mathcal{R}} [h_{\mathcal{R},1} \ \cdots \ h_{\mathcal{R},N}] + B_{\mathcal{R}}. \quad (9)$$

The matrices $W_{\mathcal{R}}$ and $B_{\mathcal{R}} = b_{\mathcal{R}}\mathbf{1}^{\top}$ define weights and biases of the classification layer.

Confer to the blue box in the lower half of Fig. 2 for a schematic representation of the relationship detection.

4. Architecture

As shown in overview figure (Fig. 2 in the main text), our proposed model includes two main parts, the object classifier and the relation predictor. In the object classifier, objects are organized as a sequence and classified with the help of the ODE Module. The relation predictor infers the predicate from visual features and semantic information which is provided by the object classifier. The object pairs are also organized as a sequence. The visual and semantic features are processed with two separate LSTM-chains, before combining and forwarding them into the ODE module.

Object Classifier The object classifier uses the raw object distributions, bounding box positions and feature maps from Faster R-CNN to predict the object classes. With a *word2vec* module, a 200-dimensional semantic embedding vector is obtained. The position embedding includes the statistical information where objects appear in images. The bounding box of the object is forwarded into a normalization layer (with momentum 0.001) and a fully connection layer with ReLU activation to obtain the 128-dimensional position embedding. These two vectors are concatenated with the feature vector resulting from compressing the $512 * 7 * 7$ -dimensional feature map to size 4096. The concatenated vector of size $200 + 128 + 4096 = 4424$ is compressed by a fully connected layer to size 1024. The result is forwarded into the ODE-module. Detection scores are computed by a fully-connected layer.

Relationship Predictor Using the union bounding box, the feature map of size $512 * 7 * 7$ is obtained. The $2 * 27 * 27$ dual masks with values in $[-0.5, 0.5]$ are forwarded into a convolution layer with 256 kernels of size $7 * 7$ and stride $2 * 2$, a max pooling layer (kernel size 3, stride 2) and another convolution layer (512 kernels with size $3 * 3$ and stride $1 * 1$) so that the output has the same size $512 * 7 * 7$ as the union box. For reducing the parameters, the output is element-wise added with the feature map of the union box. This operation combines the visual appearance and the spatial information.

The global average pooling (GAP) is applied on the $512 * 7 * 7$ feature maps of the subject box, object box and union box. the result is a 512-dimensional feature vector. Noted that we do not use fully connected layers for compression due to the large number of parameters. Using GAP avoids preparing two independent groups of FC-layers for object and union box that were used in [40]. The features of the subject, object, and union boxes are concatenated as $3 * 512$ -dimensional vectors and forwarded into a bidirectional LSTM to obtain 512-dimensional vectors of visual context.

The object classes are predicted by the Object Classifier. Based on the predicted classes, the Relation Predictor generates two 200-dimensional semantic embedding vectors corresponding subject and object for each pair. These semantic embedding vectors are concatenated and forwarded into a bidirectional LSTM to obtain 512-dimensional vectors of semantic context.

Both the visual and the semantic context vectors are concatenated and forwarded through the ODE-module. Two final fully-connected layers with ReLU-activations compute classification scores.

5. Experiments

In this section, we firstly clarify the experimental settings and implementation details. Then, we show quantitative and qualitative results on VG benchmark dataset [12] in terms of scene graph generation. We compare our results with strong prior works.

5.1. Dataset, Settings, and Evaluation

Dataset We validated our methods on the VG benchmark dataset [12] for the task of scene graph generation. However, there are varying data pre-processing strategies and dataset splits in different works. For fair comparison, we adopted the data split as described in [32] which is the most widely used. According to the data pre-processing strategy, the most-frequent 150 object categories and 50 predicate types are selected, and the training set has 75651 images while the test set has 32422 images.

Settings For the sake of fair comparison, we used Faster R-CNN [24] with VGG16 [28] as the backbone network for proposing object candidates and extracting visual feature. We adopted the code base provided by [40]. As in NeuralMotifs [40], the input image is resized to 592×592 , bounding box scales and dimension ratios are scaled, and a ROIAlign layer [7] is used to extract features within the boxes of object proposals and the union boxes of object pairs from the shared feature maps.

Evaluation There are three standard experiment settings for evaluating the performance of scene graph generation: (1) **Predicate classification** (PredCls): predict relationship labels of object pairs by giving the ground truth bounding boxes and labels of objects. (2) **Scene graph classification** (SGCls): given ground truth bounding boxes of objects, predict object labels and relationship labels. (3) **Scene graph detection** (SGDet): predict boxes, labels of object proposals and relation labels of object pairs given an image. Only when the labels of the subject, relation, and object are correctly classified, and the boxes of subject and object have more than 50% IoU with the ground truth simultaneously, it is counted as a correctly detected relationship. The most widely adopted recall@K metrics ($K = [20, 50, 100]$) for relations are used to evaluate the system performance.

Training We train our model with the sum of the cross entropy losses for objects and predicates. We collect all annotated relationships in the image and add negative relationships to keep that the relation sequences in the batch have identical length (if ground truth boxes are enough). We sample the predicates if the object pairs annotated with multiple predicates. For SGCls and SGDet, ground truth

object labels are provided to the semantic part in the training stage. For fair competition we use the same pre-trained Faster-RCNN as [40] and freeze its parameters. An ADAM optimizer was used with the batch size 6, initial learning rate 10^{-4} , and cross-entropy as loss both for object and relationship classification.

5.2. Quantitative Results and Comparison

Our results are shown in Tab. 1. The central block indicates methods that all use the same data split that is used in [32]. Two methods that use different splits are listed in the top section of the table. For MSD-net [17] in this part, we show the results reported in [40] as the authors of [17] admit the results reported in their paper cannot be reproduced using their provided code. We argue that the classes *wears* and *wearing* are *de facto* the same category (see below and the left plot in Fig. 4). Thus, the bottom section shows results for MotifNet [40] and our proposed algorithm when the relationship classes *wears* and *wearing* are merged for evaluation. However, we could not compute results for CMAT [2], since code has not been made available so far. Bold numbers indicate best results in a category, italic one second best results. It can be seen that the proposed algorithm almost consistently outperforms state-of-the-art algorithms.

Figure 4, left plot, shows a confusion matrix of the 20 most frequent relationship classes in PredCls. We immediately see that class *on* is easily confused with almost all others classes, except *has*, *wears* and *wearing*. In our opinion, this is a feature of English since the word *on* can be often used in situations in which words like *riding*, *above*, etc. can be also used. This fact is reflected in the labeling of Visual Genome. Consequently, the class *on* has significant overlap with many other classes, and can thus not be correctly distinguished. Similarly, classes *wears* and *wearing* are indistinguishable, thus all elements of class *wears* are classified to be of class *wearing*. Since they are visually identical and only differ by their grammatical function, we decided to merge both.

A confusion matrix of SGCls of the 20 most frequent object classes is shown in the right plot of Fig. 4⁵. Eye-catching is the confusion of class *man* with many other classes. Surprisingly, among these is not class *women*. Interestingly, class *man* is easily confused with classes corresponding to body parts of cloths such as *leg* or *pants*, respectively. Similarly, class *tree* has a high confusion with class *leaf* and class *building* with class *window*. This is caused, in part, by incorrectly labeled bounding boxes in the ground truth, for instance could a bounding box of the arm of a man be labeled as *man*. Furthermore, it is caused by hierarchical labeling, i.e. within a bounding box at a

⁵The confusion matrices of all the relationship classes are shown in the supplementary material.

Table 1: Comparison on VG test set [32]. All numbers in %. We use the same object detection backbone provided by [40] for fair comparison. **Bold** numbers indicate best results, *italic* ones second best results.

Methods in the middle part use the same data split as [32]. The two methods in the lower part (*merged*) use the same split as [32], but merge classes *wears* and *wearing* for evaluation. Please notice that CMAT [30] could not be evaluated in this category since code is not provided by the authors. Results for MSDN* [17] are from [40] since the authors of [17] admit that their reported results cannot be reproduced with their code.

Data Split	Method	SGGen			SGCls			PredCls		
		R@20	R@50	R@100	R@20	R@50	R@100	R@20	R@50	R@100
Others	MSDN* [17]	-	11.7	14.0	-	20.9	24.0	-	42.3	48.2
	FacNet [16]	-	13.1	16.5	-	22.8	28.6	-	-	-
[32] split	VRD [21]		0.3	0.5		11.8	14.1		27.9	35.0
	IMP [32]	14.6	20.7	24.6	31.7	34.6	35.4	52.7	59.3	61.3
	Graph R-CNN [33]	-	11.4	13.7	-	29.6	31.6	-	54.2	59.1
	Mem [30]	7.7	11.4	13.9	23.3	27.8	29.5	42.1	53.2	57.9
	MotifNet [40]	21.4	27.2	30.3	32.9	35.8	36.5	58.5	65.2	67.1
	MotifNet-Freq	20.1	26.2	30.1	29.3	32.3	32.6	53.6	60.6	62.2
	CMAT [2]	22.1	27.9	31.2	35.9	39.0	39.8	60.2	66.4	68.1
ours	21.5	27.4	30.7	36.0	39.8	40.7	58.9	66.0	67.9	
merged	MotifNet [40]	22.0	27.9	31.1	33.6	36.4	37.1	59.7	66.4	68.3
	ours	22.1	28.1	31.5	36.8	40.6	41.5	<i>60.1</i>	67.2	69.1

tree, there are other bounding boxes at leaves. The neural network then learns that these finer-grained structures are evidence for coarser classes that are semantically more general.

The mis-classifications with semantically related classes apparent in the plots shown in Fig. 4 indicate that these errors are not random effects, but provide useful information.

5.3. Ablation Studies

For ablation studies, we consider several variants of the proposed network architecture. Results are shown in Tab. 2. For model-1, we removed the ODE networks and replaced them by fully-connected layers. This measures the impact of both ODE modules. In model-2, we replaced the block for object classification in the proposed network by the classification block used in Faster R-CNN [24]. The third model shows the results using the proposed architecture. From the results of model-1, it can be seen that the overall architecture is quite powerful already. Nonetheless, when using an ODE-block for relationship classification, the already high number improve even further. When the object classification of Faster R-CNN of model-2 is replaced by an ODE-block, result for SGGen improve moderately, and those of SGCls improve about 6%. The ablation studies confirm that the proposed ODE-block is a powerful tool for semantic image understanding.

5.4. Qualitative Results

Qualitative results for scene graph generation (SGGen) are shown in Fig. 5. The images include object detections. Purple boxes denote correctly detected objects while orange boxes denote ground truth objects that are not detected. Purple edges correspond to correctly classified relationships at the R@20 setting while orange edges denote ground truth relationships that are not detected. Blue edges denote detected relationships that do not exist in ground truth annotations (false positives).

Most of the errors stem from the object detection stage. Whenever an object is not detected, relationships connecting this object are also not present in the scene graph. The cause of these errors is the Faster R-CNN detector which is exclusively used in all previous works. For comparability with state-of-the-art, we also use this detector.

There are a few false positives (blue links) which are semantically meaningful, for instance `plate-under-banana` in the upper left example. In other words, the ground truth lacks this particular relationship in such cases. Several false positives result from semantically indistinguishable classes, for example `has` and `of` in the second example from the top on the left side. In some cases as in the top left image, predicted relationships are semantically better than those in the ground truth (`banana-on-plate` vs. `plate-holding-banana`).

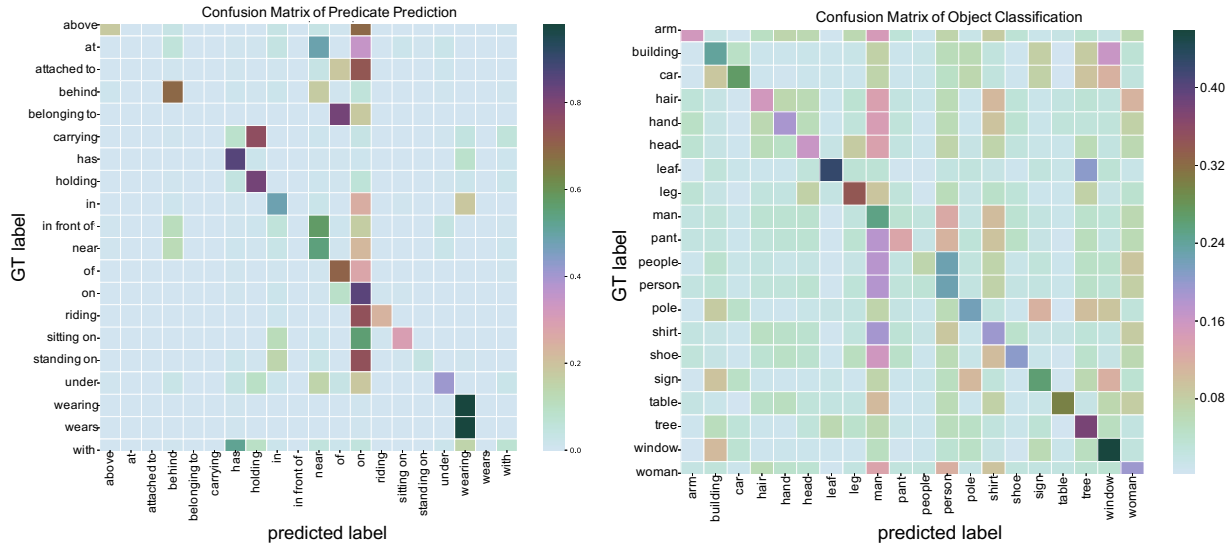


Figure 4: Left: confusion matrix of predicate prediction in PredCls setting. Right: confusion matrix of object prediction in SGCls setting. Only the top 20 frequent predicates are shown.

Table 2: Ablation studies on our model with accuracy in %. The column *object cls* specifies whether the proposed block is used for object detection or the one from Fast-RCNN [24]. The column *relationship cls* indicates if a normal fully-connected layer is used for predicate classification or the proposed module. Model-3 corresponds to the proposed architecture. It can be seen that removing the proposed ODE-module from either object classification or predicate classification has a strong, negative impact on the results. The object detection performance (mAP) follows COCO metrics [19].

Model	object cls	relationship cls	Detection	SGGen		SGCls		PredCls	
			mAP	R@50	R@100	R@50	R@100	R@50	R@100
1	FRCNN	FC	24.3	26.2	29.8	33.5	34.7	65.2	67.3
2	FRCNN	ours (ODE)	24.3	26.3	29.8	33.6	34.9	65.7	67.6
3	ours (ODE)	ours (ODE)	25.2	27.3	30.7	39.8	40.7	66.0	67.9

6. Conclusions

We presented Neural Ordinary Differential Equations for Scene Understanding (NODIS). The idea of this work is based on the fact that Mixed-Integer Linear Programs (MILP) can be used to solve problems defined by ordinary differential equations (ODEs); therefore, given any MILP, we can find a system of ODEs that can produce the solution of the MILP within a time series. Since it is not possible to manually define the system of ODE to solve, we draw on recent advances in machine learning and use a trainable function approximator instead of an explicitly defined system of ODEs. In other words, the proposed network *learns* the optimal function to solve the assignment problem, whereas previous works manually define modules to do so.

We apply this newly defined module for object classification and relationship classification. For the latter, relative improvements have decreased in the past two years. Not

surprisingly, the proposed block only causes a mediocre improvement on PredCls. In contrast, the improvement is large at task SGCls, more than 5% compared to a network not containing the ODE-block for object classification. We believe that ODE-blocks are valuable improvements for neural architectures in semantic image understanding. We will publish the code and a pre-trained model on GitHub.

References

- [1] Sanjeev Arora, Hrishikesh Khandeparkar, Mikhail Khodak, Orestis Plevrakis, and Nikunj Saunshi. A theoretical analysis of contrastive unsupervised representation learning. In *Proceedings of Machine Learning Research (PMLR)*, 2019.
- [2] Long Chen, Hanwang Zhang, Jun Xiao, Xiangnan He, Shiliang Pu, and Shih-Fu Chang. Counterfactual critic multi-agent training for scene graph generation. In *IEEE International Conference on Computer Vision (ICCV)*, pages 4613–4623, 2019.

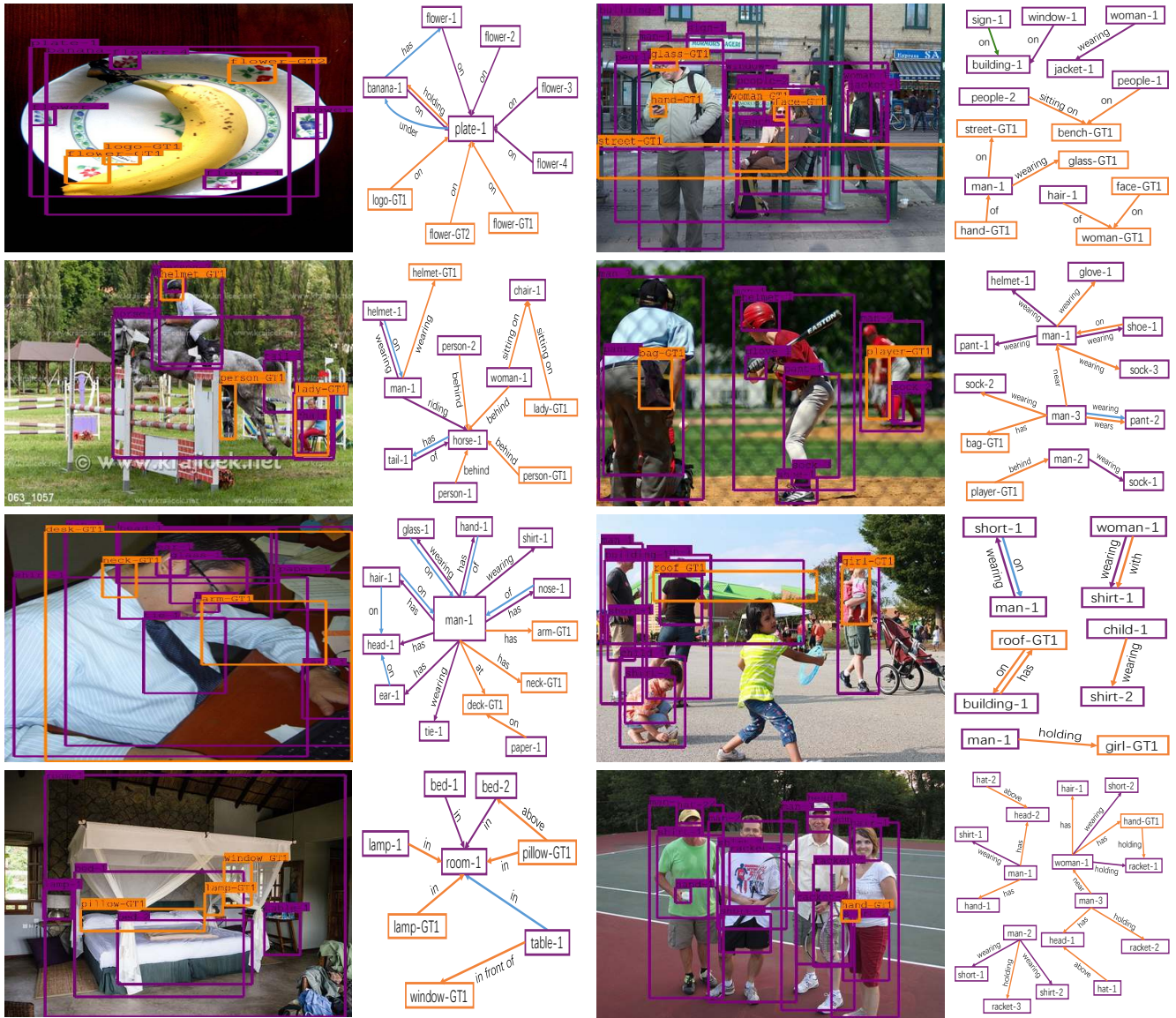


Figure 5: Qualitative results from our model in the scene graph generation setting. Purple boxes denote correctly detected objects while orange boxes denote ground truth objects that are not detected. Purple edges correspond to correctly classified relationships at the R@20 setting while orange edges denote ground truth relationships that are not detected. Blue edges denote detected relationships that do not exist in ground truth annotations (false positives).

[3] Tian Qi Chen, Yulia Rubanova, Jesse Bettencourt, and David Duvenaud. Neural Ordinary Differential Equations. In *Neural Information Processing Systems (NeurIPS)*, pages 6571–6583, 2018.

[4] Bo Dai, Yuqi Zhang, and Dahua Lin. Detecting visual relationships with deep relational networks. In *IEEE Conference on Computer Vision and Pattern Recognition (CVPR)*, pages 3076–3086, 2017.

[5] Santosh K Divvala, Derek Hoiem, James H Hays, Alexei A Efros, and Martial Hebert. An empirical study of context in object detection. In *IEEE Conference on Computer Vision*

and *Pattern Recognition (CVPR)*, pages 1271–1278, 2009.

[6] Armin Fügenschuh, Michael Herty, Axel Klar, and Alexander Martin. Combinatorial and Continuous Codels for the Optimization of Traffic Flows on Networks. *SIAM Journal on Optimization*, 16(4):1155–1176, 2006.

[7] Kaiming He, Gkioxari Georgia, Piotr Dollár, and Ross Girshick. Mask R-CNN. In *IEEE International Conference on Computer Vision (ICCV)*, pages 2961–2969, 2017.

[8] Han Hu, Jiayuan Gu, Zheng Zhang, Jifeng Dai, and Yichen Wei. Relation networks for object detection. In *IEEE Conference on Computer Vision and Pattern Recognition (CVPR)*,

- pages 3588–3597, 2018.
- [9] Justin Johnson, Ranjay Krishna, Michael Stark, Li-Jia Li, David Shamma, Michael Bernstein, and Li Fei-Fei. Image retrieval using scene graphs. In *IEEE Conference on Computer Vision and Pattern Recognition (CVPR)*, pages 3668–3678, 2015.
- [10] Thomas N Kipf and Max Welling. Semi-supervised classification with graph convolutional networks. In *International Conference on Learning Representations (ICLR)*, 2016.
- [11] Ranjay Krishna, Ines Chami, Michael Bernstein, and Li Fei-Fei. Referring relationships. In *IEEE Conference on Computer Vision and Pattern Recognition (CVPR)*, 2018.
- [12] Ranjay Krishna, Yuke Zhu, Oliver Groth, Justin Johnson, Kenji Hata, Joshua Kravitz, Stephanie Chen, Yannis Kalantidis, Li-Jia Li, David A Shamma, et al. Visual genome: Connecting language and vision using crowdsourced dense image annotations. *International Journal on Computer Vision (IJCV)*, 123(1):32–73, 2017.
- [13] Nikhil Krishnaswamy, Scott Friedman, and James Pustejovsky. Combining deep learning and qualitative spatial reasoning to learn complex structures from sparse examples with noise. In *Association for the Advancement of Artificial Intelligence (AAAI)*, volume 33, pages 2911–2918, 2019.
- [14] Lubor Ladicky, Chris Russell, Pushmeet Kohli, and Philip HS Torr. Graph cut based inference with co-occurrence statistics. In *European Conference on Computer Vision (ECCV)*, pages 239–253. Springer, 2010.
- [15] Yikang Li, Wanli Ouyang, and Xiaogang Wang. Vip-cnn: Visual phrase guided convolutional neural network. In *IEEE Conference on Computer Vision and Pattern Recognition (CVPR)*, pages 1347–1356, 2017.
- [16] Yikang Li, Wanli Ouyang, Bolei Zhou, Jianping Shi, Chao Zhang, and Xiaogang Wang. Factorizable net: an efficient subgraph-based framework for scene graph generation. In *European Conference on Computer Vision (ECCV)*, pages 346–363. Springer, 2018.
- [17] Yikang Li, Wanli Ouyang, Bolei Zhou, Kun Wang, and Xiaogang Wang. Scene graph generation from objects, phrases and region captions. In *IEEE International Conference on Computer Vision (ICCV)*, pages 1261–1270, 2017.
- [18] Xiaodan Liang, Lisa Lee, and Eric P Xing. Deep variation-structured reinforcement learning for visual relationship and attribute detection. In *IEEE International Conference on Computer Vision (ICCV)*, pages 848–857, 2017.
- [19] Tsung-Yi Lin, Michael Maire, Serge Belongie, James Hays, Pietro Perona, Deva Ramanan, Piotr Dollár, and C Lawrence Zitnick. Microsoft coco: Common objects in context. In *European Conference on Computer Vision (ECCV)*, pages 740–755. Springer, 2014.
- [20] Yong Liu, Ruiping Wang, Shiguang Shan, and Xilin Chen. Structure inference net: Object detection using scene-level context and instance-level relationships. In *IEEE Conference on Computer Vision and Pattern Recognition (CVPR)*, pages 6985–6994, 2018.
- [21] Cewu Lu, Ranjay Krishna, Michael Bernstein, and Li Fei-Fei. Visual relationship detection with language priors. In *European Conference on Computer Vision (ECCV)*, pages 852–869, 2016.
- [22] Tomas Mikolov, Kai Chen, Greg Corrado, and Jeffrey Dean. Efficient estimation of word representations in vector space. *arXiv:1301.3781*, 2013.
- [23] Varun Nagaraja, Vlad Morariu, and Larry Davis. Modeling context between objects for referring expression understanding. In *European Conference on Computer Vision (ECCV)*, pages 792–807, 2016.
- [24] Shaoqing Ren, Kaiming He, Ross Girshick, and Jian Sun. Faster R-CNN: Towards real-time object detection with region proposal networks. In *Neural Information Processing Systems (NeurIPS)*, pages 91–99, 2015.
- [25] Anna Rohrbach, Marcus Rohrbach, Ronghang Hu, Trevor Darrell, and Bernt Schiele. Grounding of textual phrases in images by reconstruction. In *European Conference on Computer Vision (ECCV)*, pages 817–834. Springer, 2016.
- [26] Jiaxin Shi, Hanwang Zhang, and Juanzi Li. Explainable and explicit visual reasoning over scene graphs. In *IEEE Conference on Computer Vision and Pattern Recognition (CVPR)*, pages 8376–8384, 2019.
- [27] Nathan Silberman, Derek Hoiem, Pushmeet Kohli, and Rob Fergus. Indoor Segmentation and Support Inference from RGBD Images. In *European Conference on Computer Vision (ECCV)*, pages 746–760, 2012.
- [28] Karen Simonyan and Andrew Zisserman. Very deep convolutional networks for large-scale image recognition. *arXiv:1409.1556*, 2014.
- [29] Damien Teney, Lingqiao Liu, and Anton van den Hengel. Graph-structured representations for visual question answering. In *IEEE Conference on Computer Vision and Pattern Recognition (CVPR)*, pages 3233–3241, 2017.
- [30] Wenbin Wang, Ruiping Wang, Shiguang Shan, and Xilin Chen. Exploring context and visual pattern of relationship for scene graph generation. In *IEEE Conference on Computer Vision and Pattern Recognition (CVPR)*, pages 8188–8197, 2019.
- [31] Yonghui Wu, Schuster Mike, Zhifeng Chen, Quoc V. Le, Mohammad Norouzi, Wolfgang Macherey, and Maxim Krikun et al. Google’s Neural Machine Translation System: Bridging the Gap between Human and Machine Translation. In *arXiv:1609.08144*, 2016.
- [32] Danfei Xu, Yuke Zhu, Christopher B Choy, and Li Fei-Fei. Scene graph generation by iterative message passing. In *IEEE Conference on Computer Vision and Pattern Recognition (CVPR)*, pages 5410–5419, 2017.
- [33] Jianwei Yang, Jiasen Lu, Stefan Lee, Dhruv Batra, and Devi Parikh. Graph r-cnn for scene graph generation. In *European Conference on Computer Vision (ECCV)*, pages 690–706, 2018.
- [34] Michael Ying Yang, Wentong Liao, Hanno Ackermann, and Bodo Rosenhahn. On support relations and semantic scene graphs. *ISPRS Journal of Photogrammetry and Remote Sensing (ISPRS)*, 131:15–25, 2017.
- [35] Xu Yang, Kaihua Tang, Hanwang Zhang, and Jianfei Cai. Auto-encoding scene graphs for image captioning. In *IEEE Conference on Computer Vision and Pattern Recognition (CVPR)*, pages 10685–10694, 2019.

- [36] Xu Yang, Hanwang Zhang, and Jianfei Cai. Shuffle-then-assemble: Learning object-agnostic visual relationship features. In *European Conference on Computer Vision (ECCV)*, pages 36–52, 2018.
- [37] Bangpeng Yao and Li Fei-Fei. Modeling mutual context of object and human pose in human-object interaction activities. In *IEEE Conference on Computer Vision and Pattern Recognition (CVPR)*, pages 17–24, 2010.
- [38] Ting Yao, Yingwei Pan, Yehao Li, and Tao Mei. Exploring visual relationship for image captioning. In *European Conference on Computer Vision (ECCV)*, pages 711–727. Springer, 2018.
- [39] Ruichi Yu, Ang Li, Vlad I Morariu, and Larry S Davis. Visual relationship detection with internal and external linguistic knowledge distillation. In *IEEE International Conference on Computer Vision (ICCV)*, pages 1974–1982, 2017.
- [40] Rowan Zellers, Mark Yatskar, Sam Thomson, and Yejin Choi. Neural motifs: Scene graph parsing with global context. In *IEEE Conference on Computer Vision and Pattern Recognition (CVPR)*, pages 5831–5840, 2018.
- [41] Ji Zhang, Kevin J. Shih, Ahmed Elgammal, Andrew Tao, and Bryan Catanzaro. Graphical contrastive losses for scene graph generation. In *arXiv:1903.02728*, 2019.
- [42] Bohan Zhuang, Lingqiao Liu, Chunhua Shen, and Ian Reid. Towards context-aware interaction recognition for visual relationship detection. In *IEEE International Conference on Computer Vision (ICCV)*, pages 589–598, 2017.
- [43] Wei Zhuo, Mathieu Salzmann, Xuming He, and Miaomiao Liu. Indoor scene parsing with instance segmentation, semantic labeling and support relationship inference. In *IEEE Conference on Computer Vision and Pattern Recognition (CVPR)*, pages 5429–5437, 2017.